

Sustainable Energy Source for Wearable Electronics Based on Multilayer Elastomeric Triboelectric Nanogenerators

*Shengming Li, Jie Wang, Wenbo Peng, Long Lin, Yunlong Zi, Sihong Wang, Gong Zhang, and Zhong Lin Wang**

Wearable electronics have attracted a wide range of attention with various functions due to the development of semiconductor industry and information technology. This work focuses on a triboelectric nanogenerator-based self-charging power system as a continuous energy source for wearable electronics. The triboelectric nanogenerator has a multilayer elastomeric structure with closely stacked arches as basic functional units. Owing to material and structural innovations, this triboelectric nanogenerator performs outstanding electric output with the maximum volume charge density $\approx 0.055 \text{ C m}^{-3}$ and practical properties for energy harvesting from body motions. Utilizing the triboelectric nanogenerator as outsole to harvest energy from walking or jogging, a pair of shoes is fabricated with the maximum equivalent charge current of each shoe being around $16.2 \mu\text{A}$ and specific fitness functions realized on each shoe separately without complex connections.

1. Introduction

With the rapid development of portable electronics and sensor networks, researchers have dedicated extensive efforts to searching for sustainable mobile energy source with the output level from μW to mW . Currently, the most commonly utilized approach is to power them by energy storage units such as batteries^[1–4] or capacitors.^[5,6] However, there are two major shortcomings. The first one is the limited lifetime, so that they cannot sustainably drive the electronics. The second one is the difficulty of disposal, which could cause serious environmental problem if not dealt with properly. As an alternative way, nanogenerators based on piezoelectric, pyroelectric, and triboelectric effects have been developed to power small electronics

sustainably solely by harvesting small-scale energy from an ambient environment.^[7–9] Among nanogenerators, triboelectric nanogenerator (TENG) has been a hot topic in recent years due to its high energy output and high conversion efficiency, with massive innovations pushing forward its development.^[10–16] In the current work, we are focusing on TENG and the corresponding power system to be the sustainable and independent energy source for small electronics. The working mechanism of a TENG is based on the coupling of triboelectrification and electrostatic induction.^[17–19] First, the physical contact of two layers of materials with distinct electron affinities creates triboelectric charges. Second, as triggered by external mechanical force, the relative separation

and contact of the triboelectric layers changes the effect of the electric field formed in the middle. As a result, free electrons flow through external circuits back and forth to achieve new balances of electrostatic charge distribution. By this means, TENG could convert mechanical energy into electricity in the external circuit. Up till now, a variety of periodical mechanical motions, such as vibrations, body motions, and ocean waves, have been utilized to trigger the motion of the TENG and to generate electric energy in the external circuit.^[11,15,20–24]

Among these different types of mechanical energy, energy from body motions (walking, arm-bending, tapping, etc.) seems to be perfect to power wearable electronic devices, since we could integrate the energy harvesting unit and the energy consumption unit together to build a self-charging power system purely based on body motions. There have been steady innovations of TENG and corresponding technologies to achieve that goal. Due to the nature of the pulsed AC output, TENGs cannot be directly used to drive most electronic devices. In the beginning, researcher turned to light-emitting diodes (LEDs) to demonstrate the output performance of their TENGs.^[21,25,26] Researchers also utilized the output signals of TENGs to fabricate self-powered sensors for body movements.^[27,28] Later, self-charging power systems based on TENGs and energy storages unit were developed to provide a regulated and manageable output.^[23,24] However, due to the restriction of the TENG's output level and the low frequency of body motions, few of the self-charging power systems could be used as continuous and independent power source for wearable electronics without external trigger at that time.^[29] Recently, with some

S. Li, Dr. J. Wang, Prof. Z. L. Wang
Beijing Institute of Nanoenergy and Nanosystems
Chinese Academy of Sciences

Beijing 100083, China

E-mail: zhong.wang@mse.gatech.edu

S. Li, Dr. J. Wang, W. Peng, Dr. L. Lin, Dr. Y. Zi,
Dr. S. Wang, Prof. Z. L. Wang
School of Materials Science and Engineering
Georgia Institute of Technology
Atlanta, GA 30332-0245, USA

S. Li, Prof. G. Zhang
Department of Mechanical Engineering
Tsinghua University
Beijing 100084, China

DOI: 10.1002/aenm.201602832



latest developments of TENGs, a few systems are capable of continuously driving wearable electronic devices solely by body motions, while the complex connections or the huge function units make them not easy to be applicable for energy harvesting from daily motions of human beings.^[30,31]

In order to further improve the output performance of TENG and to provide a practical power system as continuous power source for wearable electronics solely by daily mechanical motions, here we present an innovative multilayer elastomeric TENG and the corresponding self-charging power system. From the prospective of material and surface state, we have utilized super soft materials for both triboelectric layers and divided the large contacting surface into small sections. These technologies have been testified beneficial for the improvement of surface tribocharge density by previous works.^[31–33] As for the structure, we have designed the multilayer TENG with closely stacked basic units for each layer. No spare room has been wasted. What is more, we have emphasized the importance of volume tribocharge density for TENGs and optimized it by adjusting structural parameters based on both experimental and simulation results. These above innovations ensure the capability of TENGs to drive wearable electronics continuously and independently (without complicated connections). Apart from the high output, the TENG designed in this work also performs high system robustness, dust resistance, the ability to be washed, and the relatively high output from stretching and bending motions. These properties make our TENG-based power system practical to drive wearable electronics when integrated to clothes or shoes. Finally, we have fabricated a pair of shoes with specific fitness functions realized for each shoe solely powered by the mechanical energy harvested from walking or jogging.

2. Material Selection, Structure Design, and Process Route of the TENG

In the present work, we adopt the dielectric and conductive elastomers as the contacting layers for triboelectrification. We also utilize the conductive elastomer to be the back electrode of the TENG. The dielectric elastomer is the Ecoflex 00-30 super soft silicone, and the conductive elastomer is the mixture of Ecoflex 00-30 with carbon black and carbon nanotubes (we have presented the detailed process to manufacture the conductive elastomer in the Experimental Section) to ensure good conductivity while it is stretched. Solely fabricated by elastomeric materials, the TENG could benefit from two aspects. First, due to the flexibility and stretchability of the elastomer, we could use the TENG to extract mechanical energy from various motions, including pressing, stretching, bending, etc. Second, the super soft interfaces help improve the effective surface area for triboelectrification, which has been testified closely related to high electrical output by our previous research. According to one of our recent works, there will be barely electron transferred between two contacting materials unless the distance between them is within intermolecular distance.^[30,31]

We have also rationally designed the structure of the TENG in the present work (**Figure 1a–c**). There are plane dielectric-conductive-dielectric parts and wavy

conductive-dielectric-conductive parts overlaying each other periodically (with the thickness of the conductive layer being ≈ 0.3 mm and that of the dielectric layer being ≈ 1 mm for each part). In this way, we could divide the whole large space taken by the multilayer TENG into several layers of small arch-shaped space. Each small arch is one unit (the inset of **Figure 1b**). Considering that the units are stacked together closely without any spare space, we could utilize the whole space efficiently for high space charge density and corresponding electric current density from the TENG. What is more, since we could lengthen the plane part and flatten the wavy part for effective contact-separation, this structure is also efficient to harvest stretching mechanical energy.

For better understanding of the structure and the function of each part, here we also present the process route in **Figure 1d**. In the beginning, we fabricated several conductive elastomer films ($t_1 = 0.3$ mm in thickness) and dielectric elastomer films ($t_2 = 1$ mm in thickness) separately. For some dielectric films, we treated one side to acquire microstructures to improve contacting area (please refer to the Experimental Section for detailed procedures). Then the films were pasted together as the “conductive–dielectric–conductive” part and the “dielectric–conductive–dielectric” part. The glue was Ecoflex 00-30. Please note that the outside surfaces of the “dielectric–conductive–dielectric” parts were with microstructures. Next, we machined the acrylic sheets into frames and strips through the laser cutter as the mold to fabricate the wavy structure (the shape and size of the mold is demonstrated in **Figure S2** of the Supporting Information). We controlled the period and amplitude of the wavy part by the frame and the strips. We paved the “dielectric–conductive–dielectric” parts under the frames. Above were the “conductive–dielectric–conductive” parts and the strips. We placed the strips above or beneath the film intermittently in the position in accordance with the frame. Once the glue went dry, we removed the molds. Finally, we stacked the structures fabricated in the last step together as a multilayer TENG. The glue was Ecoflex 00-30 for connections in this work. Finally, we treated the TENG with oxygen plasma to decrease the stickiness of contacting surfaces (please refer to the Experimental Section for details). The stickiness is harmful for the high-frequency output performance.

3. Working Mechanism and Electric Output of the TENG by Pressing

Here we illustrate the working mechanism to harvest energy from pressing motions as the example. While we press the TENG firmly, contact electrification happens in the interfaces (the air gap of the arches) between the dielectric and conductive elastomers. Electrons transfer from the conductive surface to the dielectric surface because of the difference in their affinities to attract electrons (state I shown in **Figure 1e**). Later, while we reduce the pressing force, the TENG begins to recover to the original shape. Owing to electrostatic induction, electrons transfer from the back electrode of the plane part to the conductive layer of the wavy part (state II). Transferred charge amount keeps increasing until the TENG recovers to original shape (state III). Finally, when we press the TENG again, there

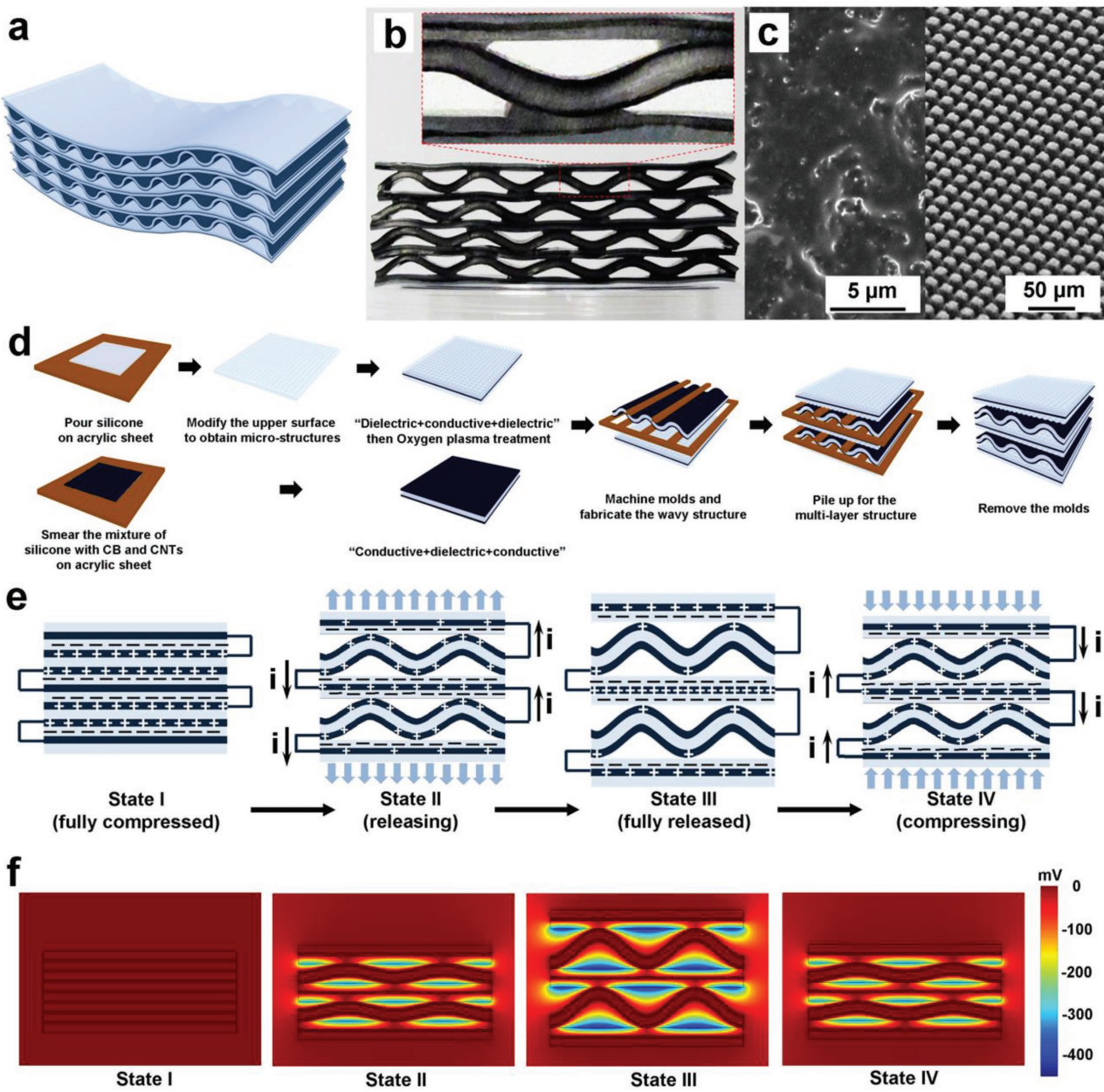


Figure 1. The structure and working mechanism of the multilayer elastomeric triboelectric nanogenerator from pressing operations. a) The 3D schematic illustration to demonstrate the structure of the triboelectric nanogenerator. b) The cross-sectional photo of the triboelectric nanogenerator. The inset is an enlarged view for one repeating unit. c) The scanning electron microscopic (SEM) images of the conductive surface (left) and the dielectric surface (right) of the triboelectric nanogenerator. d) The processing procedures to fabricate the multilayer elastomeric triboelectric nanogenerator. e,f) The electronic working mechanism (e) and corresponding potential distribution for each step while periodic pressing and releasing force is applied on the triboelectric nanogenerator with its electrodes connected in the short circuit.

is the deformation of the wavy part and same amount of electrons transfer in the opposite direction (state IV) until full contact (state I). By this means, periodic current is generated by pressing and releasing the TENG intermittently. In order to testify the mechanism, we did simulation with COMSOL. The result for each state is demonstrated in Figure 1f correspondingly, which agrees well with the above theory.

The transferred charge amount per operation cycle and the operation frequency are the two factors that fundamentally

decide the electric current into the energy storage unit. The latter factor is not a structural factor and is closely related to the mechanical motions. Therefore, we will only discuss the optimization of the former one in this part. We could express the total transferred charge amount per cycle (ΔQ_{sc}) for the multilayer TENG as

$$\Delta Q_{sc} = \Delta q(h, T) \cdot n \quad (1)$$

$$n = \frac{H}{h + 3t_1 + 3t_2} \cdot \frac{L}{T} \cdot W \quad (2)$$

where $\Delta q(h, T)$ is the transferred charge amount from one basic unit, and n is the number of basic arch-shaped units in the TENG. H , L , and W are the height, length, and width of the multilayer TENG. t_1 , t_2 are the thicknesses of the conductive layer and the dielectric layer. h , T are the maximum height of the arch-shaped air gap and the period of the wavy structure. Considering that we are expecting higher current within certain volume, maximum volume transferred charge density (ρ_{SC}) of the TENG is essential for optimized electric output but has long been ignored. Combining the above equations, ρ_{SC} could be expressed as

$$\rho_{SC} = \frac{\Delta Q_{SC}}{V} \quad (3)$$

where V is the volume of the TENG. We could calculate V according to the following equation

$$V = H \cdot L \cdot W \quad (4)$$

Combining Equations (1)–(4), we could express the volume transferred charge density as

$$\rho_{SC} = \frac{\Delta q(h, T)}{(h + 3t_1 + 3t_2) \cdot T} \quad (5)$$

In the current research, t_1 (≈ 0.3 mm) and t_2 (≈ 1 mm) are constant values. Therefore, ρ_{SC} is the function of $\Delta q(h, T)$, h , and T . We have done both experiments and finite-element simulation to investigate the relationship between the ρ_{SC} and the above parameters ($\Delta q(h, T)$, h , and T). Now that $\Delta q(h, T)$ is also necessarily relative to h and T , we only studied the effects of h and T on the electric output. We kept T constant first to investigate the effect of h onto ρ_{SC} through experiments and simulation. Next, we changed T under constant h . In this work, we adjusted h and T by changing the lateral distance and the thickness of the strips of the mold, and the lateral distance was controlled by the positioning notches on the frame.

TENGs with different H in our experiment range from 1 to 8 mm. We set T as 12 mm constantly. As shown in Figure 2b, with the increase of H , the short-circuit transferred charge amount increases from 45 to 90 nC. We could explain this tendency by the following theory. With the separation of two contacting surfaces, the electric field between those two surfaces gets weaker and a larger portion of tribocharges transferred to the back electrode. This results in the increase of ΔQ_{SC} . The area charge density for the contacting surface (σ_{SC}) follows the same trend as ΔQ_{SC} , because there is no change in the surface area for contact electrification during the increase of H . In that process, σ_{SC} increases from $95 \mu\text{C m}^{-2}$ to $190 \mu\text{C m}^{-2}$. The highest σ_{SC} value ($\approx 190 \mu\text{C m}^{-2}$) here is among the highest values ever reported.^[15,29,34,35] This may benefit from (1) contact electrification by the two soft contacting surfaces, (2) the surface area enlargement by the surface microstructures, and (3) the division of the whole large surface into several rectangular

sections. Next, we will discuss about the volume charge density (ρ_{SC}) of the TENG for it is most closely related to high electric output. As demonstrated by the experimental results in Figure 2c, with H increasing from 1 to 2.5 mm, there is the improvement of ρ_{SC} . And further growth of H results in the decrease of ρ_{SC} . We could explain the above results by the following theory. With the maximum separation distance of the two contacting layers getting larger, the percentage of transferred charges (of all tribocharges) to the back electrode increases because the electric field between the two contacting layers (and the ability to expel electrons away from the conductive layer) gets weaker, which in turn led to charge transfer from the back electrode to the contacting conductive layer. However, TENG with larger H takes up more space and there is the add-up effect for multilayer TENG. In this way, there will be fewer layers if given constant total height of the multilayer TENG. This reduces the total amount of ΔQ_{SC} for the TENG. Considering the tradeoff between these two effects, the electric output is optimized when the volume density (ρ_{SC}) reaches at its maximum value ($\approx 0.055 \text{ C m}^{-3}$). In order to testify the result that the volume density reaches at maximum when H is around 2.5 mm, we proceed finite-element simulation with COMSOL. In the simulation, we set the surface tribocharge density (σ_{SC}) as $166 \mu\text{C m}^{-2}$ and we simplify the wavy “conductive–dielectric–conductive” part to be plane when fully contacted (state I in Figure 1e) with the “dielectric–conductive–dielectric” part (without any air gap in the middle). We compare the simulation results and experimental results in Figure 2c. They agree very well with each other. Based on both experiment and simulation results, we adopt $h = 2.5$ mm as one structural parameter in our multilayer structure.

We also worked out the relationship between the electric output and the period of the wavy part (T) for one unit with both experiment and modulation. We kept H constant at 2.5 mm in both experiment and simulation. As shown in Figure 1d, the short-circuit transferred charge amount (ΔQ_{SC}) increases from 62.5 to 100 nC because the contacting area becomes larger. The surface charge density (σ_{SC}) reduces by $\approx 12.5\%$ (from ≈ 160 to $\approx 140 \mu\text{C m}^{-2}$). Next, we demonstrate the relationship between the volume density (ρ_{SC}) and the period (T) in Figure 2e according to our experiment. Since the width (W) and height (H) of the single-unit TENG remain constant, ρ_{SC} should follow the same tendency as σ_{SC} with the change of T . ρ_{SC} decreases from 0.054 C m^{-3} to 0.047 C m^{-3} in our experiment. We also prove the simulation results from COMSOL here in Figure 2e. Dissimilar to the experimental results, there is a slight improvement of ρ_{SC} with the increase of T . The opposite trends between experiment and simulation may come from the contribution of the contacting area's size. According to our previous works, smaller contacting area helps increase the effective contacting area and therefore improves the tribocharge density,^[31] and surface charge density is the basis of high electric output. In the present work, with the whole area divided into more sections and the period (T) getting smaller, there should be the increase of $\Delta \sigma_{SC}$ and ρ_{SC} . Although the decrease of T is beneficial for high output, extremely small T may lead to large curvature, which makes the wavy part difficult to deform for triboelectrification. Therefore, a rational value of T is necessary and 14 mm is used in the current structure.

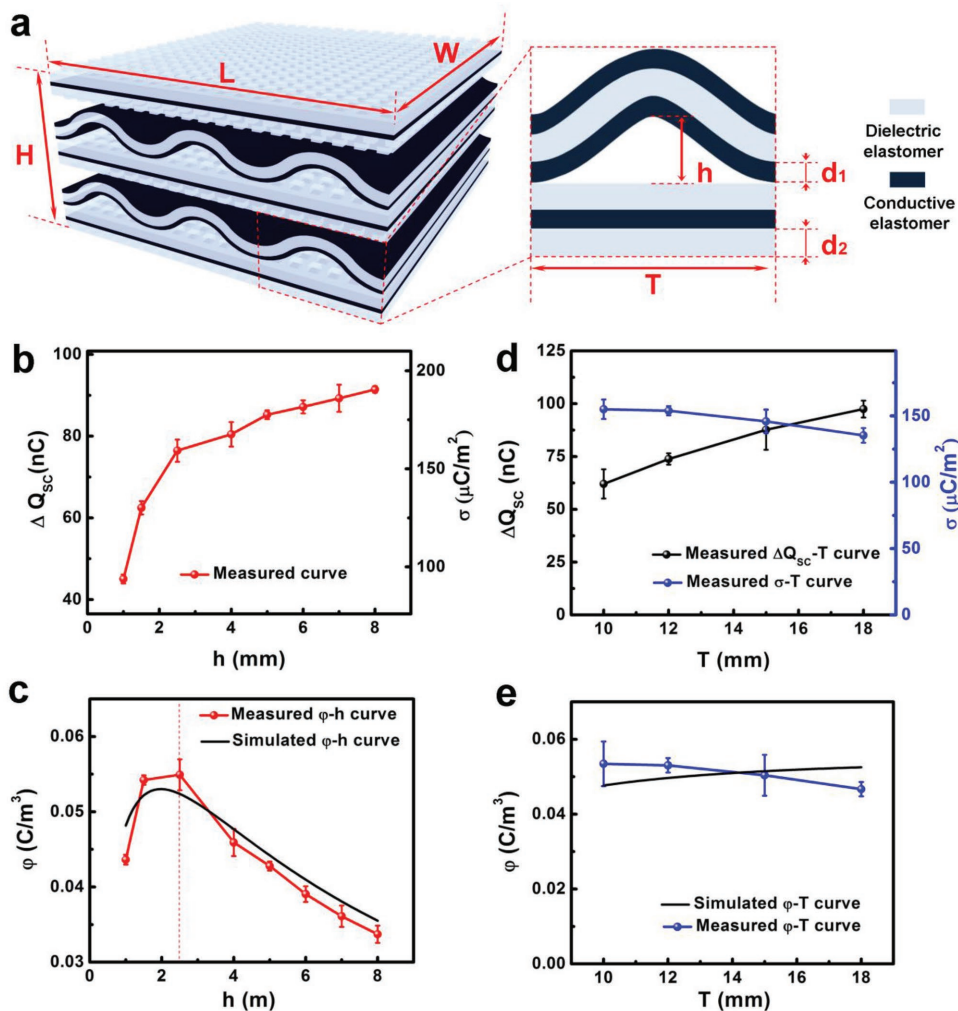


Figure 2. The structural (dimensional) optimization for the multilayer elastomeric triboelectric nanogenerator. a) The schematic illustration to show the dimensional parameters for the triboelectric nanogenerator. The inset is the enlarged schematic for a single functional unit. b) The measured short-circuit charge amount (ΔQ_{sc}) and area charge density ($\Delta \theta_{sc}$) with the increase of the maximum separation distance (h) for those basic functional units for the triboelectric nanogenerator. c) The volume charge density ($\Delta \sigma_{sc}$) with the increase of maximum separation distance (h) according to experiment and simulation. d) The measured short-circuit charge amount (ΔQ_{sc}) and area charge density ($\Delta \theta_{sc}$) with the increase of the repeating unit length (T) of the triboelectric nanogenerator. e) The volume charge density ($\Delta \sigma_{sc}$) with the repeating unit length (T) according to experiment and simulation.

We have also researched the output properties of the basic arch-shaped unit in this work. First, we testified the long-term stability of one unit. We used a shaking motor with the frequency of 8 Hz to trigger long-term contact–separation of one basic unit. As demonstrated in Figure 3a, owing to soft contact between elastomeric conductive and dielectric layers, the electric output (ΔQ_{sc}) reduces by less than 10% after 200k motion cycles. The TENG proves good robustness and long-term stability. What is more, we also examined the output property of the single arch-shaped unit under different external loads using the same shaking motor with the triggering frequency as 3 Hz. When the external load reaches at 10 Mohm, the power density maximizes at around 0.1 W m^{-2} for one arch-shaped unit. Furthermore, we illustrate the charging property for the arch-shaped units by charging an hPPy-based supercapacitor with the capacitance of 1.2 mF. As shown in Figure 3c, the charging speed becomes faster with the increase of shaking frequency.

Since there is nearly the linear relationship between the operation frequency and the charging speed, we are convinced that the TENG keeps constant output under different pressing frequencies (1–4 Hz). Figure 3d demonstrates the scale-up of multiunits. While we charge the supercapacitor with more units by pressing them under constant operation frequency (≈ 0.5 Hz), the charging speed becomes faster and there is the add-up effect with different numbers of units being pressed. This result proves that we could build up the multilayer TENG based on the arch-shaped structure (basic unit).

4. Energy Extraction from Stretching and Folding Operations

Since we fabricate the multilayer TENG solely by stretchable elastomer and the wavy part has the tendency to spread out

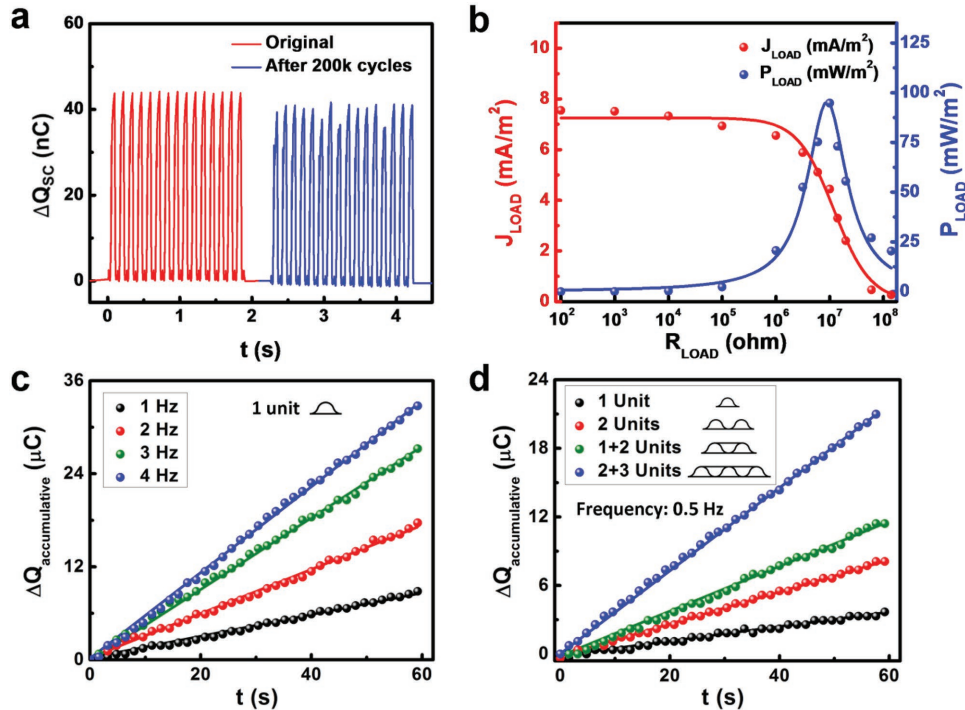


Figure 3. The output properties and charging properties for one unit of the triboelectric nanogenerators. a) The short-circuit transferred charge amount (ΔQ_{SC}) for one unit in the original condition and after ≈ 200 k pressing cycles. b) The current density (J_{LOAD}) and power density (P_{LOAD}) with different external loads (R_{LOAD}) in the circuit when pressing one unit under 3 Hz. c) The accumulated charge amount ($\Delta Q_{\text{accumulated}}$) in the supercapacitor when charged by pressing one unit of the triboelectric nanogenerator under different frequencies. d) The accumulated charge amount ($\Delta Q_{\text{accumulated}}$) in the supercapacitor when charged by pressing different number of units of the triboelectric nanogenerators concurrently under 0.5 Hz.

to be flat, the structure is also efficient to extract energy from stretching operations. The working mechanism is illustrated in Figure 4a. With the TENG being stretched/released, the conductive layers of the wavy part contact with/separate from the dielectric layers of the plane part. This causes the periodical change of the electric field in the middle and the corresponding charge transfer in the external load owing to electrostatic induction. The experimental data for one basic unit to extract energy from stretching motions is illustrated in the form of ΔQ_{SC} and V_{OC} in Figure 4b,c. In the beginning, ΔQ_{SC} increases to ≈ 10 nC and V_{OC} to ≈ 14 V because the wavy part gets flattened and the distance between the two parts becomes smaller. Further stretching the TENG could not obviously benefit the electric outputs because the conductive and the dielectric layer have already contacted each other. It should be noted that the maximum electric outputs from stretching motions are one grade smaller than those from pressing motions. During the stretching motions of the TENGs, the contact/separation is solely resulted from the flattening of the wavy part. There is no force to push together the wavy part and the flat part. Dissimilarly, for pressing operations, the contact/separation is triggered by the deformation of the wavy part. The two parts are forced together when they contact each other. More adequate contact could contribute to more tribocharges on the contacting surfaces, which in turn results in higher electric outputs (ΔQ_{SC} and V_{OC}).

We have also investigated the electric outputs by folding one basic unit in our research. Considering the structural anisotropy of the TENG, we folded one basic unit ($h = 2.5$ mm

and $T = 14$ mm) for 180° along different directions (0° , 45° , and 90°), as demonstrated in Figure 4d. We illustrate the experiment results in Figure 4e,f. The ΔQ_{SC} maximizes at ≈ 25 nC while we fold the TENG along 45° , with the ΔQ_{SC} being ≈ 12 nC and ≈ 9 nC along 0° and 90° . The V_{OC} follows a similar trend and the maximum value reaches ≈ 50 V along 45° , with smaller values for 0° and 90° (≈ 24 and ≈ 20 V). One possible explanation for the significant difference between the outputs from folding and pressing operations is that when we fold the TENG, deformation and contact electrification happens only on certain area of the surface. In comparison, periodical contact/separation happens on the whole area for pressing operation, leading to more tribo-charges per cycle. As for the change of electric output by folding along different directions, we could also explain the results by the difference in contact area, with largest area brought into contact when we fold the TENG along the direction of 45° . Although the largest folding output of the current TENG is only $\approx 30\%$ of the pressing output, it is still among the largest values to extract folding/bending mechanical energy from TENGs. Therefore, we scaled up a double-layer structure with 11 units per layer ($W = 80$ mm, $T = 12$ mm, $h = 2.5$ mm for each unit, 5 units on the top and 6 on the bottom) and connected it with an hPPy-based supercapacitor (we demonstrate the charging property of the supercapacitor in Figure S3, Supporting Information) to harvest bending mechanical energy from human beings. Bending at normal frequency, the average charging current (I_{avg}) into the supercapacitor (≈ 0 V in the beginning) is around 2.03 μ A (Figure 4g). As illustrated by Figure 4h and Video S1

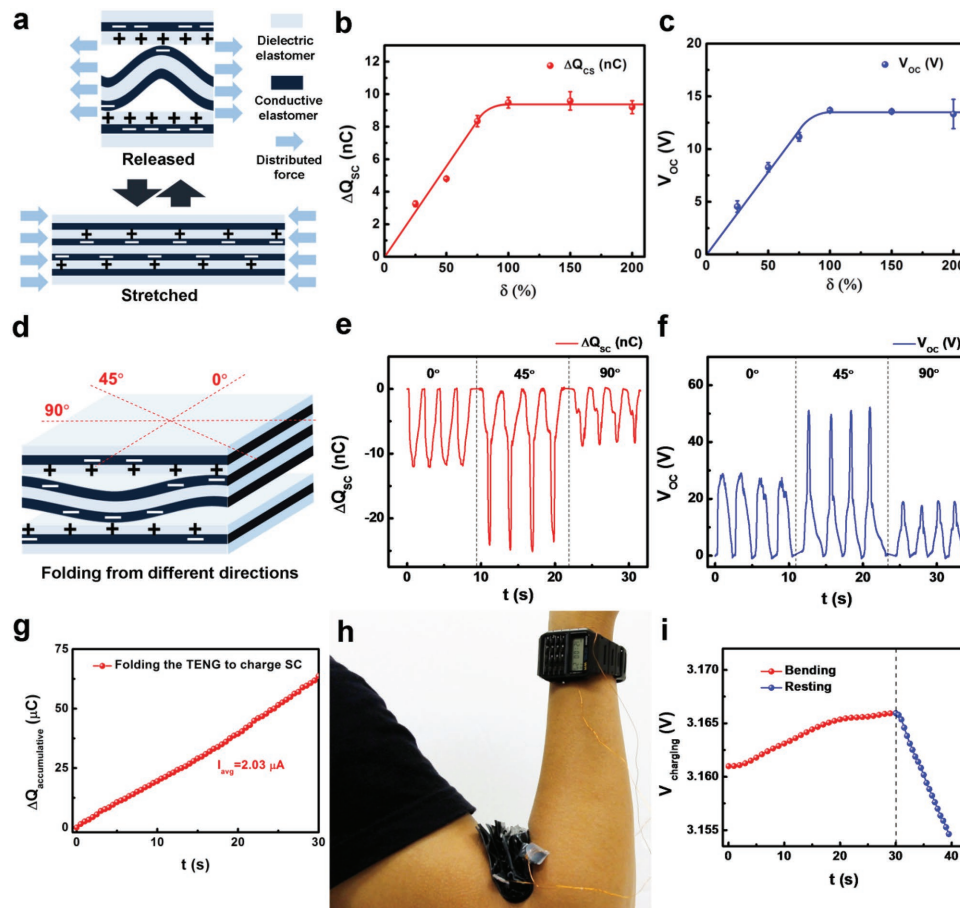


Figure 4. The electric output from one unit by stretching and folding the triboelectric nanogenerator. a) The schematic illustration to show the working mechanism for energy harvesting from stretching. The maximum b) short-circuit transferred charge amount (ΔQ_{sc}) and c) the open-circuit voltage (V_{oc}) under different elongation (δ). d) The schematic illustration to show the direction to fold the triboelectric nanogenerator. The output curves of e) short-circuit transferred charge amount (ΔQ_{sc}) and f) the open-circuit voltage (V_{oc}) with time (t). g) The accumulated charge amount (ΔQ) in the energy storage unit while bending for 180° from the direction of 90° under 2 Hz. h) The photo to illustrate that bending the triboelectric nanogenerator is able to drive an electronic watch and calculator. i) The voltage of the energy storage unit when the triboelectric nanogenerator is driving the electronic watch and calculator by bending.

(Supporting Information), the electricity generated by the TENG could sustainably power an electronic watch/calculator. We also monitored the voltage of the TENG-based self-powered system while it was sustainably powering the electronic watch/calculator. As shown in Figure 4i, the voltage keeps increasing when the supercapacitor is charged by bending arm, and there is the drastic decrease of the voltage when the arm was resting.

5. One Application of the TENG for Wearable Electronics

Considering the outstanding pressing output of the TENG in our research, we utilized the multilayer structure to fabricate shoe outsoles to harvest mechanical energy from walking or jogging. We prove the structure of the TENG-based outsole in Figure 5a. For each shoe, there are six layers of TENG in the front and six layers in the back. During the fabrication, we stacked the six layers together vertically and then tailored them into the front parts and the heel parts. Detailed

size parameters of the front part and the heel part are demonstrated in Figure S4 (Supporting Information). We selected H and T as 2.5 and 12 mm because they were optimized values. In order to resist water, dust, and humidity, we fully enclosed the TENG as well as the energy storage unit by flexible silicone rubber case. When we compress the TENG in full, the airflow from the gaps of the TENG will transfer to the surrounding space, and the case will be blown up. For this purpose, there is designed room between the case and the TENG and the case is stretchable. With the TENG-based outsole, we built a self-charging power system to extract and store energy. We utilized an hPPy-based supercapacitor with the capacitance of 1.2 mF as the energy storage unit to measure the charging performance of each shoe. As shown in Figure S5 (Supporting Information), the equivalent charging current are $\approx 6.3 \mu$ A and $\approx 6.5 \mu$ A for left and right shoes when the user walks at normal frequency, and they are $\approx 15 \mu$ A and $\approx 16.2 \mu$ A for jogging. We also present the ability of the shoes to be washed without harming the output performance in Figure S6 (Supporting Information). Thanks to the high-output performance, each shoe was built with different

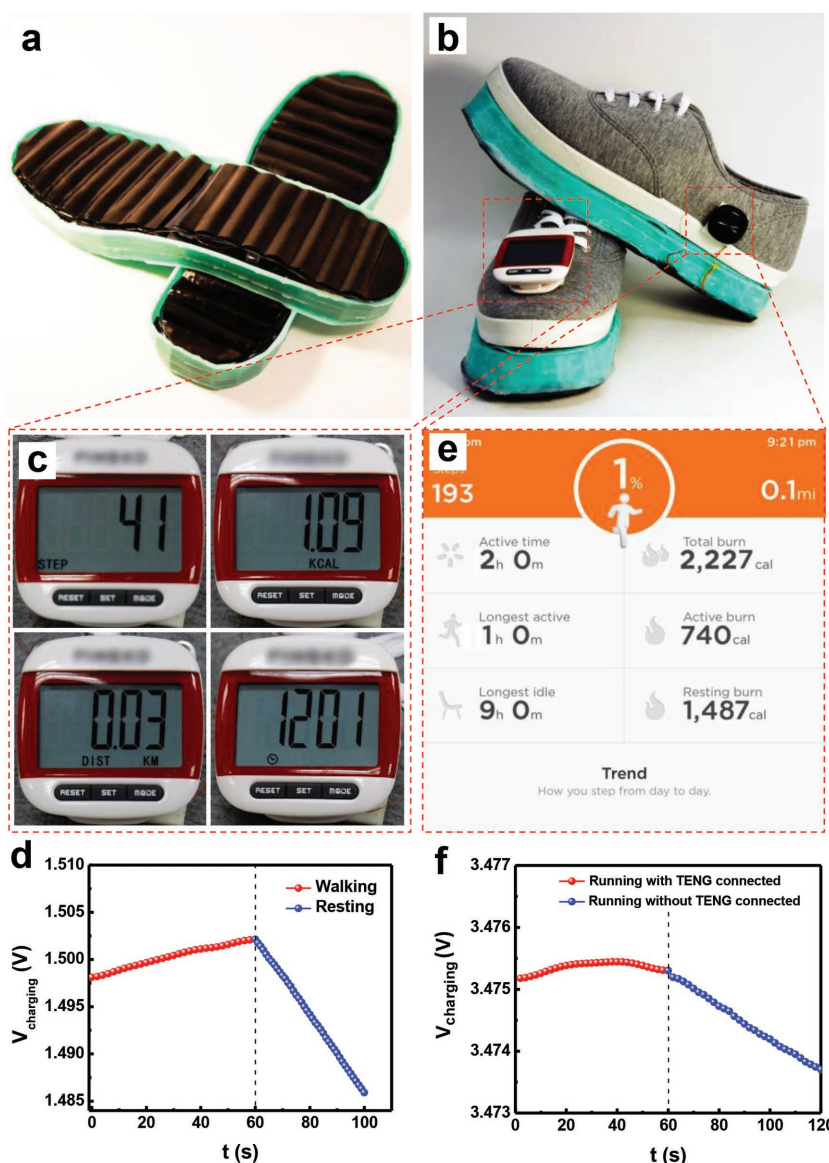


Figure 5. The demonstration of the self-powered shoes based on the multilayer elastomeric triboelectric nanogenerator and the corresponding self-charging power system. a) The photo showing the multilayer elastomeric triboelectric nanogenerator as the shoe outsoles. b) The photo showing the self-powered shoes with the function as fitness track and pedometer. The photos to demonstrate the functions of c) the pedometer and d) the fitness tracker that are powered by the triboelectric nanogenerator-based self-charging power system. The voltages of the energy storage unit while the self-charging power system is driving e) the pedometer and f) the fitness tracker.

electronic fitness device to realize specific fitness function. We have demonstrated the circuit diagrams of energy consuming electronics integrated with the energy harvesters and energy storage devices on the shoes in Figure S7 (Supporting Information). As demonstrated in Figure 5b,c, we added a portable digital multipedometer on the left shoe. It could display time, count walking steps, measure walking distance, and calculate the calories burnt. The energy storage unit is an hPPy-based supercapacitor with the capacitance of 12 mF. The charging/discharging curve of the supercapacitor is demonstrated in Figure S8 (Supporting Information). Figure 5d and Video S2 (Supporting Information) illustrate that while the operator

walks at normal frequency, electric energy collected from his left shoe could power the multipedometer continuously, and there is also spare energy stored in the supercapacitor. In this way, his left shoe could record daily fitness data without external power source. Dissimilar to the left shoe, the right shoe was implanted with the fitness tracker to record and store exercise data, which was proved in Figure 5b. The energy storage unit for the self-charging power system is a lithium-ion battery (PGEB021212 by PowerStream, and the charging property of the lithium-ion battery is shown in Figure S8 of the Supporting Information). When the user was jogging, the fitness tracker was driven continuously and the exercise information was recorded and stored in the cell phone (Video S3, Supporting Information). Figure 5f testifies that the TENG-based self-powered system on the right shoe could solely power the fitness tracker sustainably, in which the potential maintains at the constant level when the TENG charges the lithium-ion battery (LIB), while it decreases dramatically without the TENG connected. The function of the right shoe is to provide more accurate exercise data that could be directly updated and stored in the cell phone. To sum up, we have fabricated a pair of fitness shoes with different functions for each shoe without external power supply.

6. Conclusions

In summary, we present a sustainable power source to continuously power wearable electronics solely based on material-and-structure-optimized elastomeric TENG. From the prospective of material and surface state, all-elastomer-based structure with super soft conductive and dielectric layers for triboelectrification has been adopted, and the large surface for triboelectrification has been divided into small sections. From the structural aspect, we have designed the multilayer TENG with closely stacked basic units

for each layer. This is accomplished by layering up the plane “dielectric-conductive-dielectric” part and the wavy “conductive-dielectric-conductive” part. Moreover, we have adjusted the structural parameters based on both experimental and simulation results for the output optimization of each arch. Based on these innovations, we have achieved outstanding electric output of the TENG from pressing motions with maximized volume charge density as $\approx 0.055 \text{ C m}^{-3}$. On the other hand, there is also relatively high output from stretching and bending motions, which is capable of driving an electronic watch continuously and independently. Apart from the output, the multilayer TENG in this work also performs high system robustness, and it is

dust and water resistant when fully enclosed. These properties make the TENG-based power system practical to drive wearable electronics when integrated to clothes or shoes. Finally, we have fabricated a pair of shoes with specific fitness functions for each shoe continuously realized solely driven by the TENG-based self-charging power system. The left shoe could record daily fitness data through a multipedometer and the right shoe could record exercise data and transfer these into a cell phone through a fitness tracker.

7. Experimental Section

Fabrication of the Conductive Elastomer: The base and cure (1:1 by volume ratio) of the silicone rubber (Ecoflex 00-30) were mixed in a beaker to acquire silicone rubber. Then the mixture of conductive carbon black and CNTs (2:1 by weight ratio) was added into the liquid and the liquid was stirred until uniformly mixed. The volume ratio of the silicone rubber (Ecoflex 00-30) and the carbon black was 1:1 (with the weight ratio of the CNTs, the carbon black, and the silicone rubber being 1:2:26.8). Next, the carbon black/CNTs@silicone rubber was smeared onto a piece of acrylic plate. Please note that the plate was preprocessed with a release agent. After the mixture was cured at a temperature of 30 °C for 5 h, a conductive elastomer was obtained.

Fabrication of the Micropatterned Structures on the Surface Dielectric Elastomer: A silicon wafer was patterned with the array of squares with a typical photolithography process as the mold. Then the wafer was preprocessed with release agent. Next, the liquid Exoflex 00-30 base-and-cure mixture was poured on the top until it went dry (30 °C for 5 h). Finally, the dielectric elastomer was peeled off from the silicon wafer.

Oxygen Plasma Treatment of the Multilayer TENG: The "Hummer V" by Anatech was utilized for the oxygen plasma treatment for the multilayer TENG. The dielectric layer was treated for 5 min at 4 V. During this process, the vacuum degree of the chamber was around 1 mtorr.

Fabrication of the hPPy-Based Supercapacitor: The supercapacitor was fabricated as a symmetrical structure with two hPPy electrodes as positive and negative electrodes. 1 M KCl aqueous solution was used as electrolyte. Finally, the supercapacitor was packaged by two pieces of Kapton films in sandwich structure. The synthesis process of the hPPy is discussed below. Pyrrole monomer (Py, Capchem, 99%) was twice distilled prior to use. The polymerization solution contained 300×10^{-3} M pyrrole, 100×10^{-3} M *p*-toluenesulfonic acid (TOSH, China Medicine Group, AR), and 400×10^{-3} M sodium *p*-toluenesulfonic (TOSNa, China Medicine Group, CP). The electrodeposition was proceeded in a three-electrode cell with titanium sheet as working electrode and counter electrode, and a saturated calomel electrode (SCE) as refer electrode. The hPPy films were deposited on titanium electrodes by a pulse potentiostatic method. The parameters for the pulse are a high potential of 0.75 V versus SCE, a high potential period of 0.04 s, a low potential of -0.2 V versus SCE, and a low potential period of 0.12 s.

Supporting Information

Supporting Information is available from the Wiley Online Library or from the author.

Acknowledgements

S.L., J.W., and W.P. contributed equally to this work. This research was supported by the "thousands talents" program for pioneer researcher and his innovation team, China, the National Key R&D Project from Minister of Science and Technology (2016YFA0202704), and the National Natural Science Foundation of China (Grant Nos. 51432005, 5151101243, 51561145021, and 21274115).

Received: December 20, 2016

Revised: January 18, 2017

Published online: February 17, 2017

- [1] B. Dunn, H. Kamath, J. M. Tarascon, *Science* **2011**, *334*, 928.
- [2] B. Huskinson, M. P. Marshak, C. Suh, S. Er, M. R. Gerhardt, C. J. Galvin, X. Chen, A. Aspuru-Guzik, R. G. Gordon, M. J. Aziz, *Nature* **2014**, *505*, 195.
- [3] Z. Q. Peng, S. A. Freunberger, Y. H. Chen, P. G. Bruce, *Science* **2012**, *337*, 563.
- [4] J. B. Goodenough, K. S. Park, *J. Am. Chem. Soc.* **2013**, *135*, 1167.
- [5] M. F. El-Kady, V. Strong, S. Dubin, R. B. Kaner, *Science* **2012**, *335*, 1326.
- [6] Y. Zhu, S. Murali, M. D. Stoller, K. J. Ganesh, W. Cai, P. J. Ferreira, A. Pirkle, R. M. Wallace, K. A. Cychosz, M. Thommes, D. Su, E. A. Stach, R. S. Ruoff, *Science* **2011**, *332*, 1537.
- [7] Z. L. Wang, J. H. Song, *Science* **2006**, *312*, 242.
- [8] X. Wang, J. Song, J. Liu, Z. L. Wang, *Science* **2007**, *316*, 102.
- [9] Y. Zi, L. Lin, J. Wang, S. Wang, J. Chen, X. Fan, P. K. Yang, F. Yi, Z. L. Wang, *Adv. Mater.* **2015**, *27*, 2340.
- [10] Z. L. Wang, *ACS Nano* **2013**, *7*, 9533.
- [11] P. Bai, G. Zhu, Y. Liu, J. Chen, Q. Jing, W. Yang, J. Ma, G. Zhang, Z. L. Wang, *ACS Nano* **2013**, *7*, 6361.
- [12] L. Lin, S. Wang, Y. Xie, Q. Jing, S. Niu, Y. Hu, Z. L. Wang, *Nano Lett.* **2013**, *13*, 2916.
- [13] Z. L. Wang, *Faraday Discuss.* **2014**, *176*, 9533.
- [14] S. Wang, L. Lin, Z. L. Wang, *Nano Energy* **2014**, *11*, 436.
- [15] S. Wang, Y. Xie, S. Niu, L. Lin, C. Liu, Y. S. Zhou, Z. L. Wang, *Adv. Mater.* **2014**, *26*, 6720.
- [16] S. Li, S. Wang, Y. Zi, Z. Wen, L. Lin, G. Zhang, Z. L. Wang, *ACS Nano* **2015**, *9*, 7479.
- [17] Z. L. Wang, J. Chen, L. Lin, *Energy Environ. Sci.* **2015**, *8*, 2250.
- [18] S. Niu, Y. Liu, S. Wang, L. Lin, Y. S. Zhou, Y. Hu, Z. L. Wang, *Adv. Mater.* **2013**, *25*, 6184.
- [19] S. Niu, Z. L. Wang, *Nano Energy* **2014**, *14*, 161.
- [20] S. Wang, S. Niu, J. Yang, L. Lin, Z. L. Wang, *ACS Nano* **2014**, *8*, 12004.
- [21] Z. Wen, H. Guo, Y. Zi, M. H. Yeh, X. Wang, J. Deng, J. Wang, S. Li, C. Hu, L. Zhu, Z. L. Wang, *ACS Nano* **2016**, *10*, 6526.
- [22] H. Guo, Z. Wen, Y. Zi, M. H. Yeh, J. Wang, L. Zhu, C. Hu, Z. L. Wang, *Adv. Energy Mater.* **2016**, *6*, 1501593.
- [23] S. Li, W. Peng, J. Wang, L. Lin, Y. Zi, G. Zhang, Z. L. Wang, *ACS Nano* **2016**, *10*, 7973.
- [24] J. Wang, X. Li, Y. Zi, S. Wang, Z. Li, L. Zheng, F. Yi, S. Li, Z. L. Wang, *Adv. Mater.* **2015**, *27*, 4830.
- [25] P. Bai, G. Zhu, Z. H. Lin, Q. Jing, J. Chen, G. Zhang, J. Ma, Z. L. Wang, *ACS Nano* **2013**, *7*, 3713.
- [26] F. Yi, X. Wang, S. Niu, S. Li, Y. Yin, K. Dai, G. Zhang, L. Lin, Z. Wen, H. Guo, J. Wang, M. H. Yeh, Y. Zi, Q. Liao, Z. You, Y. Zhang, Z. L. Wang, *Sci. Adv.* **2016**, *2*, e1501624.
- [27] B. Hwang, J. Lee, T. Trung, E. Roh, D. Kim, S. Kim, N. Lee, *ACS Nano* **2015**, *9*, 8801.
- [28] S. Jung, J. Lee, T. Hyeon, M. Lee, D. Kim, *Adv. Mater.* **2014**, *26*, 6329.
- [29] G. Zhu, J. Chen, T. Zhang, Q. Jing, Z. L. Wang, *Nat. Commun.* **2014**, *5*, 487.
- [30] S. Niu, X. Wang, F. Yi, Y. S. Zhou, Z. L. Wang, *Nat. Commun.* **2015**, *6*, 37.
- [31] J. Wang, S. Li, F. Yi, Y. Zi, J. Lin, X. Wang, Y. Xu, Z. L. Wang, *Nat. Commun.* **2016**, *7*, 12744.
- [32] Y. S. Zhou, S. Li, S. Niu, Z. L. Wang, *Nano Res.* **2016**, *9*, 3705.
- [33] S. Li, Y. S. Zhou, Y. Zi, G. Zhang, Z. L. Wang, *ACS Nano* **2016**, *10*, 2528.
- [34] Y. Zi, S. Niu, J. Wang, Z. Wen, W. Tang, Z. L. Wang, *Nat. Commun.* **2015**, *6*, 8376.
- [35] W. Tang, T. Jiang, F. R. Fan, A. F. Yu, C. Zhang, X. Cao, Z. L. Wang, *Adv. Funct. Mater.* **2015**, *25*, 3718.